
Deep Physics Prior for First Order Inverse Optimization

Haoyu Yang Kamyar Azizzadenesheli Haoxing Ren
 NVIDIA Research
 {haoyuy, kamyara, haoxingr}@nvidia.com

Abstract

Inverse design optimization aims to infer system parameters from observed solutions, posing critical challenges across domains such as semiconductor manufacturing, structural engineering, materials science, and fluid dynamics. The lack of explicit mathematical representations in many systems complicates this process and makes the first order optimization impossible. Mainstream approaches, including generative AI and Bayesian optimization, address these challenges but have limitations. Generative AI is computationally expensive, while Bayesian optimization, relying on surrogate models, suffers from scalability, sensitivity to priors, and noise issues, often leading to suboptimal solutions. This paper introduces Deep Physics Prior (DPP), a novel method enabling first-order gradient-based inverse optimization with surrogate machine learning models. By leveraging pretrained auxiliary Neural Operators, DPP enforces prior distribution constraints to ensure robust and meaningful solutions. This approach is particularly effective when prior data and observation distributions are unknown.

1 Introduction

Inverse design optimization addresses the challenge of identifying objectives or parameters (f) based on observed solutions (u^*), making it a fundamental approach in various real-world scenarios across multiple disciplines. For example, in structural engineering, inverse design is used to infer the location and extent of damage based on sensor data. In chip design, inverse lithography plays a critical role in optimizing chip patterns to improve manufacturability. Similarly, in materials science, it is employed to identify atomic or molecular structures that yield desired properties, such as thermal conductivity or elasticity. Aerodynamics also relies on inverse optimization for airfoil design, among other applications. These examples highlight the wide-reaching impact of inverse design across diverse fields.

Limitations of MCMC. Solving inverse optimization problems typically requires access to a surrogate model that approximates the forward behavior of the system. These models are often queried using approaches like Bayesian optimization or Markov Chain Monte Carlo (MCMC) Cotter et al. (2013). However, surrogate models frequently rely on finite element analysis or rigorous simulations, which are computationally expensive. To address these challenges, data-driven generative AI methods have garnered significant research attention. Among these, the Fourier Neural Operator (FNO) has emerged as a state-of-the-art solution, demonstrating a remarkable $400\times$ speed-up over traditional surrogate models for solving physics-based inverse problems Li et al. (2021). Despite its advantages, FNO-based methods inherit the limitations of MCMC, such as heuristic-based exploration and neglecting the underlying physics of the problem. Moreover, MCMC fails to leverage the differentiable nature of FNO, further limiting its potential.

Limitations of Generative Model. Another common approach is to train a generative AI model to directly predict the inverse solution Yang et al. (2020); Huang et al. (2024); Long & Zhe (2024);

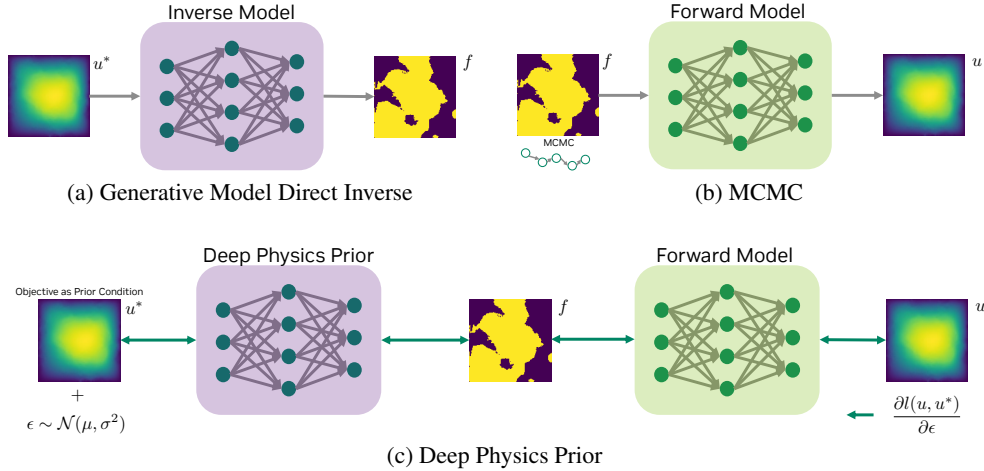


Figure 1: Comparison of inverse design optimization schemes. (a) Data-driven generative model that maps objectives to parameters. (b) Determine inverse solution using Markov-Chain Monte Carlo (MCMC) through pre-trained surrogate model. (c) Derive inverse solution using first-order optimization on system parameters constrained by a deep physics prior.

Yang & Ren (2024). However, the performance of such models heavily depends on the underlying data distribution. As shown in Section 4, when the training data consists of mixed distributions, the generative model tends to approximate a weighted average of these distributions. Consequently, the predicted inverse solutions are noisy and require additional fine-tuning or optimization to achieve satisfactory results.

Why Not First Order Optimization? First-order optimization leverages gradient information to efficiently navigate toward the solution, enabling significantly faster convergence compared to the random-walk behavior of MCMC. With operator learning providing a differentiable surrogate forward model, it becomes theoretically feasible to use gradient propagation to infer the desired inverse solution Azizzadenesheli et al. (2024). However, this approach is not as straightforward as it may seem. The FNO family, as a backbone of data-driven neural networks, is **differentiable but highly susceptible to adversarial examples**. Consequently, gradient-based methods often generate out-of-distribution inverse solutions, effectively creating adversarial examples.

Our Contributions. We propose Deep Physics Prior (DPP), a novel methodology for solving inverse design problems using first-order optimization with only a data-driven surrogate model. DPP integrates a forward Fourier Neural Operator (FNO) as the surrogate model and an auxiliary FNO as a physics prior to mitigate adversarial example generation. The key contributions of this work are as follows:

- **FNO-Based Advantages:** DPP inherits the strengths of FNO, including resolution invariance and support for free super-resolution, making it highly versatile for various inverse design tasks.
- **Purely Data-Driven Approach:** DPP is a fully data-driven methodology, particularly effective for problems with unknown data distributions or when explicit and accurate mathematical formulations are unavailable.
- **Superior Performance in Case Studies:** Through extensive experiments on 2D Darcy Flow, we demonstrate that DPP significantly outperforms alternative approaches. Specifically, it achieves a 68.5% smaller relative error compared to direct generative AI methods while maintaining high computational efficiency. For the inverse lithography problem, our method outperforms SOTA numerical optimizer with 21 \times smaller edge placement violation and 10 \times speedup.

2 Related Works

Fourier Neural Operator. FNO Li et al. (2021) is a data-driven learning approach that solves partial differential equations in a discretized domain. The key component is iterative representation updates through the kernel integral operators computed in the Fourier domain. Each integral layer is given by

$$v_{t+1}(\mathbf{x}) = \sigma(\mathcal{F}^{-1}(R_\phi \cdot (\mathcal{F}v_t))(\mathbf{x}) + \mathcal{W}v_t(\mathbf{x})), \forall \mathbf{x} \in D, \quad (1)$$

where v_t and v_{t+1} denotes the input and the output function of each layer, σ is some nonlinear activation that is applied on the integral operator at Fourier domain and a linear transformation \mathcal{W} , and R_ϕ is the Fourier transform of the integral kernel parameterized by some neural networks. The FNO family is inherently resolution-agnostic, providing efficient global perception. It has proven effective both as a PDE solver and as a surrogate model for practical applications. However, FNOs remain vulnerable to adversarial attacks, which hinder their use for differentiable inverse design. In this paper, we explore the feasibility of leveraging pretrained surrogate models for first-order inverse design optimization.

GAN and GANO. Generative Adversarial Networks (GANs) Goodfellow et al. (2014a) are among the most successful paradigms for generative learning, particularly in performing unsupervised data analysis in finite-dimensional spaces. A GAN consists of two components: a generator, which maps a Gaussian latent space to the data space, and a discriminator, which distinguishes between the synthetic data distribution and the true observed data distribution. Generative Adversarial Neural Operator (GANO) Rahman et al. (2022) extends the GAN framework to infinite-dimensional function spaces by replacing the generator and discriminator with neural operator layers and constructing the training guidance in function spaces. This extension enables GANO to map from one Gaussian random field (GRF) to the data distribution, effectively generating data in infinite-dimensional spaces. It is important to note that both GANs and GANOs rely on the assumption of a known data distribution, which they use during training to distinguish and generate samples effectively.

Adversarial Sampling. Adversarial attacks have become a significant area of research since the rise of deep learning Goodfellow et al. (2014b), with a focus on improving the robustness and security of deep learning models. A key insight from this body of work is that all data-driven deep learning models are vulnerable to adversarial examples due to the discrete nature of training data and model overparameterization. This vulnerability poses a significant challenge when applying pretrained surrogate models for inverse design tasks. A recent study Liu et al. (2023) explores this phenomenon through an adversarial data augmentation framework called LADA. LADA is designed to generate chip design layouts likely to fail the predictions of pretrained manufacturing simulation models. Using a GAN-based framework, chip design images are produced, and gradient ascent is applied to backpropagate gradients to the input of the GAN’s generator during the generation process. Remarkably, the generated chip designs successfully induce failures in the surrogate simulation model while preserving the characteristics of true chip design distributions. This study empirically demonstrates the potential of GANs to act as structural constraints for generating adversarial data, offering new insights into the interplay between adversarial attacks and data-driven surrogate models.

PINN. Physics-informed neural networks (PINNs) Raissi et al. (2019) have gained significant attention in recent years for their ability to solve partial differential equations (PDEs) by incorporating physical laws into the learning process. The development of PINNs offers a promising framework to balance between data-driven learning and physics-based modeling, enabling more generalizable and interpretable machine learning models for real-world applications. However, several challenges remain, including issues with convergence, sensitivity to inaccurate or incomplete governing equations, and high computational cost—particularly when solving complex or stiff PDEs.

3 The Methodology

3.1 Problem Formulation

Forward Operator. Let \mathcal{A} denote the input function space and \mathcal{U} denote the output function space. The corresponding forward operator is $\mathcal{F} : \mathcal{A} \rightarrow \mathcal{U}$, maps any function $a : \mathcal{D}_{\mathcal{A}} \rightarrow \mathbb{R}^n$ in \mathcal{A} to a

function $u = \mathcal{F}(a)$, where $u : \mathcal{D}_{\mathcal{U}} \rightarrow R^{n'}$. To approximate \mathcal{F} , in this work, we adopt the Fourier Neural Operators (FNOs), learned using supervised data pairs (a, u) , where $a \sim \mathcal{P}_{\mathcal{A}}$ and u is the corresponding solution in the forward operator. The FNO takes the input of a discretized function a and outputs a prediction $F_{\theta}(a) \approx \mathcal{F}(a)$.

Inverse Design. The inverse problem is defined as recovering a such that $\mathcal{F}(a)$ matches a desired target response u^* . Typically, inverse mapping is ill-posed and underdetermined, especially when the true forward operator \mathcal{F} arises from nonlinear physics-based simulation, such as PDE solvers. To address this challenge, we propose a data-driven approach that (1) approximates \mathcal{F} using a learned neural operator, and (2) constrains the inverse problem using a generative model that captures the prior distribution of realistic designs.

3.2 Adversarial Behavior of F_{θ} in Inverse Design

The goal of inverse design optimization is to find $a^* = \arg \min_{a \in \mathcal{A}} \|\mathcal{F}(a) - u^*\|^2$ where \mathcal{F} is typically expensive and we approximate this with $\hat{a} = \arg \min_{a \in \mathcal{A}} \|F_{\theta}(a) - u^*\|^2$. However, this approximation might lead to a significant optimization error, considering

$$\begin{aligned} \|\mathcal{F}(a) - u^*\|^2 &= \|F_{\theta}(a) + \Delta(a) - u^*\|^2 \\ &= \underbrace{\|F_{\theta}(a) - u^*\|^2}_{\text{Operator Approximation}} + \underbrace{2 \langle F_{\theta}(a) - u^*, \Delta(a) \rangle + \|\Delta(a)\|^2}_{\text{Residual}}, \end{aligned} \quad (2)$$

where $\Delta(a) = \mathcal{F}(a) - F_{\theta}(a)$ refers to the surrogate error. Clearly, minimizing $\|F_{\theta}(a) - u^*\|^2$ does not necessarily minimize the inverse objective $\|\mathcal{F}(a) - u^*\|^2$ unless $\Delta(a) \approx 0$. However, $\Delta(a)$ could be large when $a \notin \text{supp}(\mathcal{P}_{\mathcal{A}})$. This explains the existence of adversarial designs a such that $\|F_{\theta}(a) - u^*\|^2 \ll \|\mathcal{F}(a) - u^*\|^2$. We will show such an effect in Table 1, where an extremely large error occurs when performing maximum likelihood estimation (MLE) on the inverse solution.

3.3 Deep Physics Prior

To address the bad approximation of F_{θ} , we define a generative model on function space \mathcal{A} , as an operator \mathcal{G} mapping random input function q drawn from \mathcal{N} , a predefined Gaussian random field (GRF) on \mathcal{A} , to samples $a = \mathcal{G}(q)$ in function space \mathcal{A} . The operator \mathcal{G} is trained such that the sample functions a , i.e., $a \sim \mathcal{G}_{\#}\mathcal{P}_{\mathcal{A}}$, represent the distribution $\mathcal{P}_{\mathcal{A}}$. We train \mathcal{G} following GANO framework, using the relaxed dual representation of the Wasserstein distance in function spaces. In paralytically, \mathcal{G} is trained using the following objective function,

$$\min_{\mathcal{G}} \max_d \mathbb{E}_{a \sim \mathcal{P}_{\mathcal{A}}} [d(a)] - \mathbb{E}_{a \sim \mathcal{G}_{\#}\mathcal{P}_{\mathcal{A}}} [d(a)] + \lambda \mathbb{E}_{a \sim \mathcal{P}'_{\mathcal{A}}} [(\|\partial d(a)\|_{\mathcal{A}^*} - 1)^2], \quad (3)$$

where d is a discriminator neural functional $d : \mathcal{A} \rightarrow \mathbb{R}$ with Fréchet derivative operator ∂d on the function space \mathcal{A} with \mathcal{A}^* denoting the dual space. In this relaxation, $\mathcal{P}'_{\mathcal{A}} = r\mathcal{G}_{\#}\mathcal{P}_{\mathcal{A}} + (1-r)\mathcal{P}_{\mathcal{A}}$ for r as samples from the uniform distribution in $[0, 1]$. Similar to the forward operator, we assume a discretized approximation of \mathcal{G} to be G_{ϕ} .

In the inverse problem, we are often given the noisy observation of function u , and we are after sampling function a from its posterior. After training both \mathcal{F} and \mathcal{G} , in order to sample from the posterior, we propose running Langevin dynamics on the space input to the generative model G to sample functions a using the following dynamics

$$q \leftarrow q - \gamma \partial(\|u - \mathcal{F}(G(q))\|^2 + \lambda \|q\|^2) + \sqrt{2\gamma} \mathcal{N}. \quad (4)$$

with γ representing the learning rate. The sample generated by the above dynamics represent the Laplace approximation of posterior. In this work we run this dynamics on space of q since Langevin dynamics assume Gaussian prior and space of q has GRF prior. For the maximum a posteriori estimation(MAP), we run the above dynamics with no noise to recover the MAP.

3.4 Inverse Design Error Analysis

We measure the quality of the inverse design through the error between the forward response of the inverse design and the desired value:

$$\mathcal{L}(a) = \|\mathcal{F}(a) - u^*\|. \quad (5)$$

To derive an analysis of the inverse design through deep physics prior, we make the following lemma:

Lemma 1. Let $\hat{a} = G_\phi(q^*)$ and $q^* = \arg \min_q \|\mathcal{F}_\theta(G_\phi(q)) - u^*\|$ is the inverse optimization solution from Langevin dynamics. The inverse design quality from the deep physics prior is upper-bounded by

$$\mathcal{L}(\hat{a}) \leq \mathcal{L}(a^*) + L_F \epsilon_G + 2\epsilon_F, \quad (6)$$

assuming

1. There exists $a^* \in \mathcal{A}$ such that $a^* = \arg \min_{a \in \mathcal{A}} \mathcal{L}(a)$ and the generator approximates a^* via q^* such that $\|G_\phi(q^*) - a^*\| \leq \epsilon_G$.
2. F_θ is L_F -Lipschitz.
3. The forward operator approximate the true forward model with error $\|\mathcal{F}(a) - F_\theta(a)\| \leq \epsilon_F, \forall a \in \text{range}(G_\phi)$.

Lemma 1 gives a fundamental practical design guidance of deep physics prior that improving the generalization capability of the forward operator leads to smaller gap between the inverse optimization results and the golden inverse solution.

4 Experiments

In this section, we compare our deep physics prior methodology with several representative inverse design solutions on two time-independent case studies including 2D Darcy FFlow and Semiconductor lithography. All experiments are conducted on a single NVIDIA RTX A6000 Ada with 48GB memory.

4.1 Inverse Darcy Flow

The Darcy flow equation is a second-order elliptic partial differential equation (PDE) given by:

$$\begin{aligned} -\nabla \cdot (u(x) \nabla f(x)) &= k(x), & x \in (0, 1), \\ f(x) &= 0, & x \in \partial(0, 1), \end{aligned} \quad (7)$$

where $f(x)$ represents the flow pressure to be solved, $u(x)$ is the permeability field, and $k(x)$ is the forcing function. The Darcy equation models various physical systems, including fluid transport through porous media, elasticity in materials, and heat conduction. For simplicity, we set $k(x) = 1$ for all $x \in [0, 1]$, and discretize both the permeability field and the flow pressure into 2D matrices, $\mathbf{A}, \mathbf{U} \in \mathbb{R}^{N \times N}$, respectively.

Following Li et al. (2021), we define a parameterized surrogate model $F(\cdot; \mathbf{w}_s)$ that approximates the mapping from the discretized permeability field to the flow pressure, i.e., $\mathbf{A} \rightarrow \mathbf{U}$. The inverse problem is then formulated as recovering the permeability field given a flow pressure profile, i.e., $\mathbf{U} \rightarrow \mathbf{A}$.

Dataset. In Li et al. (2021), the permeability field is sampled from a Gaussian random field (GRF) distribution:

$$\mathbf{A} \sim \psi_{\#} \mathcal{N}(\mathbf{0}, (-\Delta + \tau^2 \mathbf{I})^{-\alpha}), \quad (8)$$

where Δ is the Laplacian with Neumann boundary conditions, and τ and α are parameters controlling the correlation structure of the field. Larger values of α result in smoother fields, while larger τ values correspond to more correlated, large-scale structures. To ensure the ellipticity of the Darcy coefficients, a transformation $\psi : \mathbb{R} \rightarrow \mathbb{R}$ is applied to the sampled field. Two common choices for ψ are:

- A clipping function Li et al. (2021):

$$\psi(x) = \begin{cases} 12, & \text{if } x \geq 0, \\ 4, & \text{otherwise.} \end{cases} \quad (9)$$

- An exponentiation function Rahman et al. (2022):

$$\psi(x) = e^x. \quad (10)$$

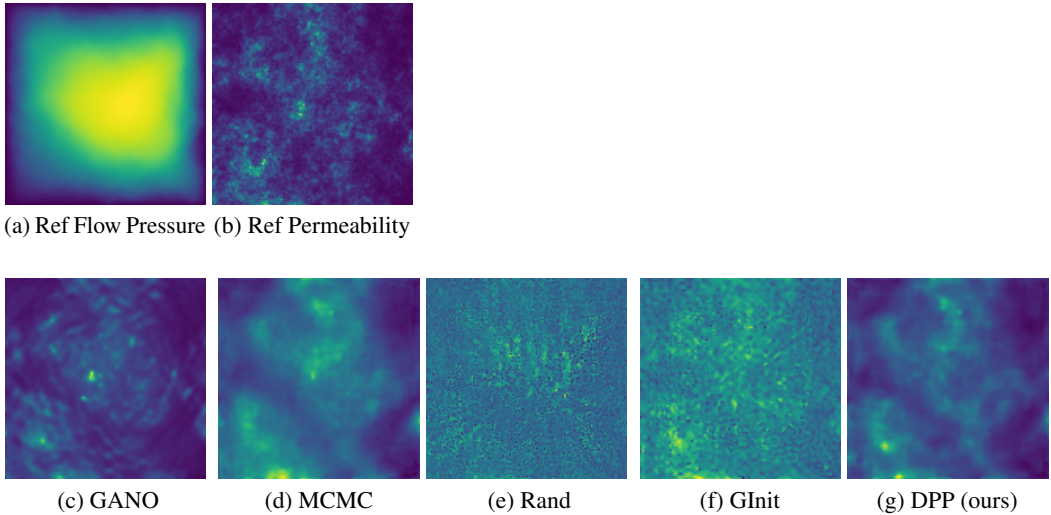


Figure 2: Visualization of inverse Darcy flow with exponentiated Permeability.

For our experiments, we generate two variants of the Darcy dataset using both transformation methods, allowing us to evaluate our framework’s ability to handle both binary and continuous permeability distributions. Unlike Li et al. (2021), where data is generated with fixed τ and α , we introduce additional variability by sampling $\alpha \sim \mathcal{U}(1, 2.5)$, making the problem more challenging. For both the continuous and clipped cases, we generate 6000 samples for training the surrogate and prior models and an additional 100 samples for inverse optimization.

Model Architecture and Training. Both the forward surrogate model $F(\mathbf{A}; \mathbf{w}_s)$ and the generative prior model $G(\mathbf{U} + \epsilon; \mathbf{w}_p)$ are defined with four Fourier layers, 32 channels, and 25 maximum truncated modes. Both F and G are trained for 50 epochs using cosine annealing scheduler with a starting learning rate 0.1. During the inverse optimization, we assume the expected flow pressure to be \mathbf{U}^* and both \mathbf{w}_s and \mathbf{w}_p are frozen. We use Prodigy optimizer Mishchenko & Defazio (2023) for the inverse optimization and have a maximum of 100 iterations.

Results. Table 1 presents the inverse design results on the 2D Darcy Flow. The columns “Continuous” and “Clipped” correspond to two dataset variants based on different choices of ψ . The relative error (“Rel Error”) and maximum error (“Max Error”) are computed between the predicted pressure field \mathbf{U} and the ground truth \mathbf{U}^* . We compare four baseline methods with our proposed approach. “GANO” refers to a generative adversarial neural operator Rahman et al. (2022) trained to directly map observations to inverse solutions. “MCMC (FNO)” employs Markov-Chain Monte Carlo using a Fourier Neural Operator as the surrogate forward model F , combined with the No-U-Turn sampler Hoffman et al. (2014). “Rand” and “GInit” are gradient-based optimization methods that descend through a pretrained surrogate model; the former initializes \mathbf{A} randomly, while the latter uses the output of a pretrained generative model. “DPP” is our method, which incorporates a deep physics prior into the optimization process. Our method achieves the lowest Rel Error and Max Error among all baselines. Notably, “DPP” reaches accuracy comparable to “MCMC (FNO)” while offering a $20\times$ speedup. Visualization examples are also available in Figure 2 and Figure 3, where we can observe without prior model, first order inverse optimization will likely fail due to adversarial examples (see Figure 2(e) and Figure 3(e)). Also, direct inverse from generative model tries to capture the average distribution from the entire training dataset, yielding a smoother output (see Figure 2(c) and Figure 3(c)).

4.2 Inverse Lithography

AI has greatly benefited from advances in chip design and manufacturing, which are fundamentally enabled by photolithography—a critical process that transfers circuit patterns onto silicon wafers.

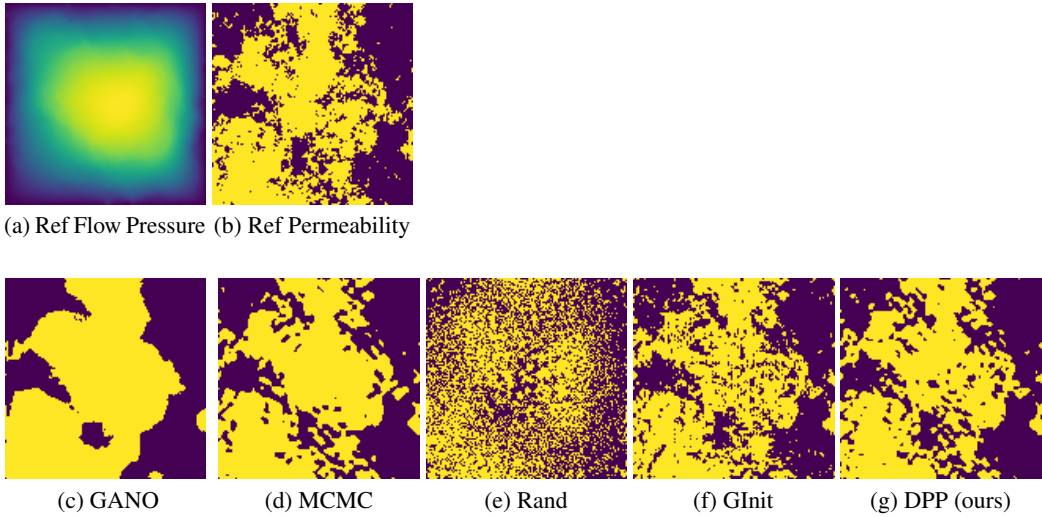


Figure 3: Visualization of inverse darcy flow with clipped permeability.

Table 1: Inverse Design on 2D Darcy Flow.

Method	Continuous		Clipped		Throughput (s)
	Rel Error	Max Error	Rel Error	Max Error	
GANO	0.037	0.507	0.035	0.087	0.003
MCMC (FNO)	0.038	0.477	0.011	0.042	179
Rand	0.876	757	0.052	0.133	22.7
GInit	0.134	9.416	0.013	0.058	22.7
DPP (ours)	0.023	0.236	0.011	0.034	9.16

However, due to the growing mismatch between the resolution limits of lithography systems and the ever-decreasing feature sizes in modern integrated circuits, significant pattern distortion can occur during the design-to-wafer transfer process Yang & Ren (2024); Banerjee et al. (2013); Zheng et al. (2023). To mitigate these distortions, design optimization is essential prior to manufacturing, ensuring that the final wafer pattern accurately reflects the intended layout.

This pattern transfer process is often referred to as forward lithography, which can be approximated by the following optical imaging model:

$$\mathbf{I} = \sum_{k=1}^N \alpha_k \|\mathbf{h}_k \otimes \mathbf{M}\|^2, \quad (11)$$

where \mathbf{M} denotes the input mask pattern (to be optimized), \mathbf{I} is the resulting light intensity distribution on the wafer, and α_k , \mathbf{h}_k represent lithography system parameters capturing the physics of light propagation and mask interaction. The photoresist coating on the wafer responds to the light intensity distribution, forming the final printed pattern. This resist process is typically modeled using a thresholding operation:

$$\mathbf{Z}(i, j) = \begin{cases} 1, & \text{if } \mathbf{I}(i, j) > I_{\text{th}}, \\ 0, & \text{otherwise.} \end{cases} \quad (12)$$

where \mathbf{Z} denotes the binary wafer pattern and I_{th} is the intensity threshold.

The inverse lithography (ILT) problem then aims to determine an optimized mask \mathbf{M} such that the resulting wafer pattern \mathbf{Z} closely matches the target design \mathbf{Z}^* . As semiconductor technology progresses into the sub-nanometer regime, the lithographic models grow increasingly complex, and the calibration of model parameters (e.g., α_k , \mathbf{h}_k) becomes highly labor-intensive. Consequently,

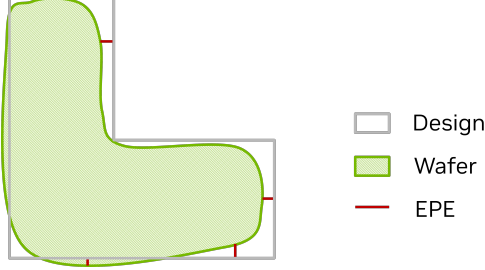


Figure 4: Measurement of inverse lithography performance using edge placement error.

data-driven approaches are becoming indispensable for scalable and accurate lithography modeling and optimization.

To quantify the discrepancy between the target pattern Z^* and the simulated wafer pattern Z , a widely used metric is the Edge Placement Error (EPE). EPE is defined as the minimum distance from predefined sampling points on the target design Z^* to the nearest corresponding horizontal or vertical edge on the printed pattern Z , as illustrated in Figure 4. These sampling points are typically specified based on technology node requirements. If the EPE at any sampling point exceeds a predefined threshold, it is considered an EPE violation, indicating that the printed feature may not meet functional or yield specifications. The total number of EPE violations across the layout serves as a key evaluation metric for assessing the quality of the lithographic patterning and the effectiveness of the mask optimization.

Dataset. We employ LithoBench Zheng et al. (2023) as our evaluation benchmark. The training data contains over 100K triplets of chip design clips Z^* , masks from numerical optimizer M , and simulated intensity images I . The benchmark suit also contains real-world design data from the Nangate45 standard cell library from OpenRoad Flow Ajayi et al. (2019), which will be used to evaluate our solutions on inverse lithography problems.

Model Architecture and Training. We still use the standard Fourier neural operator for the forward surrogate model $F(\cdot; \mathbf{w}_s)$ with 35 maximum truncated modes and 64 channels. For the inverse lithography task, it is more challenging to have suitable inverse prior model. For simplicity and fair result comparison, we pick $G(\cdot; \mathbf{w}_p)$ the backbone model Convolution FNO from ILILT Yang & Ren (2024). In particular, F takes the input of mask images M and output the corresponding UV intensity map I , and G takes the input of design target Z^* and outputs estimated mask image prior M . We have the same optimizer settings as Darcy experiment during inverse lithography optimization except we allow a maximum of 200 optimization steps.

Results. We compare our results against state-of-the-art (SOTA) inverse lithography techniques and report the numerical outcomes in Table 2. The method “MultiILT” represents a SOTA numerical ILT solver Sun et al. (2023), which directly computes gradients from Equation (11) and Equation (12). As previously discussed, numerical solvers face significant challenges at advanced technology nodes due to the high computational cost of evaluating the forward and backward passes, which require frequent Fourier transforms over high-dimensional image data. The method “ILILT” adopts a data-driven strategy by formulating ILT as an implicit layer learning problem. We evaluate two different model sizes of “ILILT” for comparison. Similarly, “GANO” is a generative adversarial neural operator that learns a functional mapping from the chip design space to the optimized mask space. “DPP” denotes our proposed method. Note that we do not include other baselines such as MCMC, Rand, or GInit (as used in Inverse Darcy Flow), because ILT is a more complex and sensitive task, and these baselines fail to produce meaningful results. Overall, our method achieves the lowest number of EPE violations among all methods. Although “GANO” achieves the highest throughput, it suffers from $28\times$ more EPE violations, which can severely compromise chip functionality and manufacturing yield.

Figure 5 illustrates the benefits of DPP through comparison with the legacy numerical optimizer (MultiILT), where we show that the legacy solver exhibits missing components after the inverse lithography optimization while DPP successfully produces high fidelity masks with good wafer image. This can be explained by the fact that using Fourier Neural Operator as a surrogate model for aerial

Table 2: Inverse Lithography.

Method	EPE Violation	Throughput (s)
MultiILT (Numerical Solver)	0.21	4
ILILT-130K	0.25	0.4
ILILT-45M	0.08	0.8
GANO	0.28	0.06
DPP (ours)	0.01	0.4

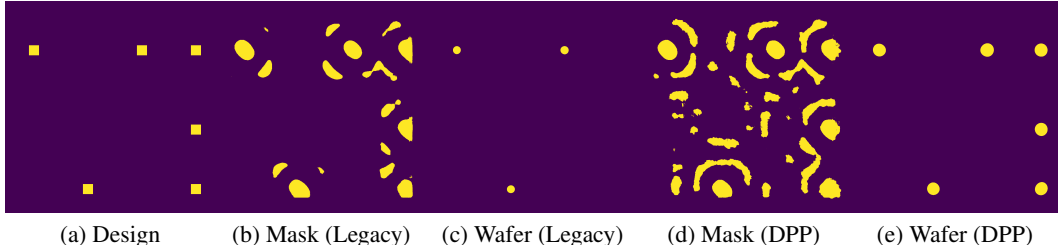


Figure 5: Visualization of inverse lithography solutions. (a) Snippet of the chip design. (b) The optimized mask of (a) using legacy numerical optimization. (c) The wafer image of (b). (d) The optimized mask using DPP. (e) The wafer image of (d).

image prediction can effectively constrain the ILT optimization onto a learned surrogate manifold, significantly simplifying the search space and enabling more efficient convergence compared to traditional Hopkin’s diffraction model-based ILT.

5 Conclusion and Discussion

In this paper, we propose Deep Physics Prior, a data-driven methodology for first-order inverse design optimization. By jointly learning a forward surrogate operator F_θ that approximates the physical forward mapping $\mathcal{F} : \mathcal{A} \rightarrow \mathcal{U}$, and a generative model G_ϕ that maps latent variables q to the design space \mathcal{A} , we enable differentiable, efficient, and physically consistent inverse optimization. We validate our approach on two representative applications: inverse design in 2D Darcy flow and mask optimization for inverse lithography. In both cases, our method produces higher-quality solutions and demonstrates greater robustness compared to existing state-of-the-art techniques.

Deep Physics Prior presents a promising paradigm for solving inverse problems in complex scientific and engineering domains where physical models are governed by partial differential equations or expensive black-box simulations. By leveraging data-driven surrogates and generative priors, this framework bridges the gap between physical fidelity and optimization tractability. Our approach has broad implications for scientific computing, enabling scalable and interpretable inverse design in areas such as fluid dynamics, materials discovery, and microelectronics. It promotes a shift toward learning-based design methodologies that respect physical priors and domain constraints.

The effectiveness of our method depends on the quality of both the forward surrogate and the generative model, which introduces a trade-off between optimization accuracy and model capacity. Poorly trained models may lead to degraded performance or unrealistic designs. Future research directions include extending the framework to unstructured domains (e.g., graphs or meshes), incorporating uncertainty quantification into the design loop, and applying the method to more diverse and real-world inverse design tasks.

References

Ajayi, T., Blaauw, D., Chan, T.-B., Cheng, C.-K., et al. OpenRoad: Toward a self-driving, open-source digital layout implementation tool chain. In *Proceedings of Government Microcircuit Applications and Critical Technology Conference*, 2019.

Azizzadenesheli, K., Kovachki, N., Li, Z., Liu-Schiaffini, M., Kossaifi, J., and Anandkumar, A. Neural operators for accelerating scientific simulations and design. *Nature Reviews Physics*, 6(5): 320–328, 2024.

Banerjee, S., Li, Z., and Nassif, S. R. ICCAD-2013 CAD contest in mask optimization and benchmark suite. In *IEEE/ACM International Conference on Computer-Aided Design (ICCAD)*, pp. 271–274, 2013.

Cotter, S., Roberts, G., Stuart, A., and White, D. Mcmc methods for functions: Modifying old algorithms to make them faster. *Statistical Science*, 28(3):424–446, 2013.

Goodfellow, I., Pouget-Abadie, J., Mirza, M., Xu, B., Warde-Farley, D., Ozair, S., Courville, A., and Bengio, Y. Generative adversarial nets. *Advances in neural information processing systems*, 27, 2014a.

Goodfellow, I. J., Shlens, J., and Szegedy, C. Explaining and harnessing adversarial examples. *arXiv preprint arXiv:1412.6572*, 2014b.

Hoffman, M. D., Gelman, A., et al. The no-u-turn sampler: adaptively setting path lengths in hamiltonian monte carlo. *Journal of Machine Learning Research (JMLR)*, 15(1):1593–1623, 2014.

Huang, J., Wu, Y., Wang, F., Fang, Y., Nan, Y., Alkan, C., Abraham, D., Liao, C., Xu, L., Gao, Z., et al. Data-and physics-driven deep learning based reconstruction for fast mri: Fundamentals and methodologies. *IEEE Reviews in Biomedical Engineering*, 2024.

Li, Z., Kovachki, N., Azizzadenesheli, K., Liu, B., Bhattacharya, K., Stuart, A., and Anandkumar, A. Fourier neural operator for parametric partial differential equations. *International Conference on Learning Representations (ICLR)*, 2021.

Liu, M., Yang, H., Khailany, B., and Ren, H. An adversarial active sampling-based data augmentation framework for ai-assisted lithography modeling. In *IEEE/ACM International Conference on Computer-Aided Design (ICCAD)*, pp. 1–9, 2023.

Long, D. and Zhe, S. Invertible fourier neural operators for tackling both forward and inverse problems. *arXiv preprint arXiv:2402.11722*, 2024.

Mishchenko, K. and Defazio, A. Prodigy: An expeditiously adaptive parameter-free learner. *arXiv preprint arXiv:2306.06101*, 2023.

Rahman, M. A., Florez, M. A., Anandkumar, A., Ross, Z. E., and Azizzadenesheli, K. Generative adversarial neural operators. *arXiv preprint arXiv:2205.03017*, 2022.

Raissi, M., Perdikaris, P., and Karniadakis, G. E. Physics-informed neural networks: A deep learning framework for solving forward and inverse problems involving nonlinear partial differential equations. *Journal of Computational Physics*, 378:686–707, 2019.

Sun, S., Yang, F., Yu, B., Shang, L., and Zeng, X. Efficient ilt via multi-level lithography simulation. In *2023 60th ACM/IEEE Design Automation Conference (DAC)*, pp. 1–6. IEEE, 2023.

Yang, H. and Ren, H. Ililt: Implicit learning of inverse lithography technologies. In *International Conference on Machine Learning (ICML)*, 2024.

Yang, H., Li, S., Deng, Z., Ma, Y., Yu, B., and Young, E. F. Y. GAN-OPC: Mask optimization with lithography-guided generative adversarial nets. *IEEE Transactions on Computer-Aided Design of Integrated Circuits and Systems (TCAD)*, 2020.

Zheng, S., Yang, H., Zhu, B., Yu, B., and Wong, M. D. Lithobench: Benchmarking ai computational lithography for semiconductor manufacturing. In *Conference on Neural Information Processing Systems (NIPS)*, 2023.